4-11-2023

STING-dependent interferon signatures restrict osteoclast differentiation and bone loss in mice

Susan MacLauchlan
Brigham and Women's Hospital
Priyanka Kushwaha
Brigham and Women's Hospital
Albert Tai
Tufts University School of Medicine
Sijia Chen
Brigham and Women's Hospital
Catherine Manning
Brigham and Women's Hospital

See next page for additional authors

Recommended Citation

MacLauchlan, Susan; Kushwaha, Priyanka; Tai, Albert; Chen, Sijia; Manning, Catherine; Swarnkar, Gaurav; Abu-Amer, Yousef; Fitzgerald, Katherine A; Sharma, Shruti; and Gravallese, Ellen M, "STING-dependent interferon signatures restrict osteoclast differentiation and bone loss in mice." Proceedings of the National Academy of Sciences of the United States of America. 120, 15. e2210409120 (2023). https://digitalcommons.wustl.edu/oa_4/2031

PNAS RESEARCH ARTICLE | IMMUNOLOGY AND INFLAMMATION

STING-dependent interferon signatures restrict osteoclast differentiation and bone loss in mice

Susan MacLauchlan[a], Priyanka Kushwaha[a], Albert Tai[b], Sijia Chen[a], Catherine Manning[a], Gaurav Swarnkar[c], Yousef Abu-Amer[c], Katherine A. Fitzgerald[d], Shruti Sharma[b,1], and Ellen M. Gravallese[a,1]

Edited by Judy Lieberman, Harvard Medical School, Boston, MA; received June 22, 2022; accepted February 14, 2023

Stimulator of interferon genes (STING) is a key mediator of type-I interferon (IFN-I) signaling in response to a variety of stimuli, but the contribution of STING to homeostatic processes is not fully characterized. Previous studies showed that ligand activation of STING limits osteoclast differentiation in vitro through the induction of IFNβ and IFN-I interferon-stimulated genes (ISGs). In a disease model (SAVI) driven by the V154M gain-of-function mutation in STING, fewer osteoclasts form from SAVI precursors in response to receptor activator of NF-kappaB ligand (RANKL) in an IFN-I-dependent manner. Due to the described role of STING-mediated regulation of osteoclastogenesis in activation settings, we sought to determine whether basal STING signaling contributes to bone homeostasis, an unexplored area. Using whole-body and myeloid-specific deficiency, we show that STING signaling prevents trabecular bone loss in mice over time and that myeloid-restricted STING activity is sufficient for this effect. STING-deficient osteoclast precursors differentiate with greater efficiency than wild types. RNA sequencing of wild-type and STING-deficient osteoclast precursor cells and differentiating osteoclasts reveals unique clusters of ISGs including a previously undescribed ISG set expressed in RANKL naïve precursors (tonic expression) and down-regulated during differentiation. We identify a 50 gene tonic ISG signature that is STING dependent and shapes osteoclast differentiation. From this list, we identify interferon-stimulated gene 15 (ISG15) as a tonic STING-regulated ISG that limits osteoclast formation. Thus, STING is an important upstream regulator of tonic IFN-I signatures shaping the commitment to osteoclast fates, providing evidence for a nuanced and unique role for this pathway in bone homeostasis.

interferon | osteoimmunology | bone homeostasis | STING

Significance

Baseline expression of type I interferons (IFN-I) and IFN-I-stimulated genes (ISGs), termed "tonic IFN," regulates cellular homeostasis. IFN-Is inhibit the formation of osteoclasts, yet neither the transcriptional profile of ISGs in osteoclast precursors, nor upstream regulators of tonic IFN in osteoclastogenesis, is known. We reveal that tonic IFN-I expression characterizes osteoclast precursors prior to receptor activator of NF-kappaB ligand (RANKL) exposure and that many tonic ISGs are repressed by RANKL signaling. In addition, the ISG response to RANKL is complex and multifaceted. We show that the immune signaling adaptor stimulator of interferon genes (STING) induces the expression of many tonic ISGs in osteoclast precursors and preserves bone mass. This study provides unique avenues for therapeutic modulation of bone.

Bone volume is strictly regulated via homeostatic mechanisms that maintain bone strength, integrity, and systemic availability of calcium (1). Myeloid-derived, bone-resorbing osteoclasts and mesenchymal-derived, bone-forming osteoblasts allow for the maintenance of bone volume (1). Excess activity of osteoclasts leads to pathologic bone loss, as seen in postmenopausal osteoporosis, autoimmune arthritis, and periodontitis (1). This underscores the necessity for regulating the bone-eroding activity of osteoclasts to maintain bone homeostasis. Osteoclastogenesis leads to terminal differentiation of osteoclast precursors into mature, multinucleated, bone-resorbing osteoclasts upon exposure to the cytokine receptor activator of NF-kappaB ligand (RANKL), signaling through its receptor RANK. In vitro, osteoclastogenesis is recapitulated by exposure of M-CSF-expanded osteoclast precursors (RANKL naïve) to RANKL, resulting in multinuclear cell formation over a period of several days (2, 3). RANKL-stimulated cells proceed through well-defined stages, including the acquisition of osteoclast-specific genes and upregulation of requisite surface markers to achieve the fusogenic state, followed by cell–cell fusion (4). These stages provide multiple opportunities for regulating osteoclastogenesis, with many positive regulators described for each stage. However, few negative regulators of osteoclastogenesis have been elucidated. Of the key negative regulators identified for osteoclastogenesis, the type I interferon (IFN-I) cytokine family is foremost.

The IFN-I family of cytokines is a pleiotropic, complex family regulating the cell-intrinsic immune response and is comprised of IFNβ and 14 IFNα family members (5). Two main findings have shaped our understanding of IFN-I in osteoclastogenesis: the increased capacity of IFNα/β receptor (IFNAR1)-deficient cells to form mature osteoclasts from osteoclast precursors and the concomitant decrease in bone volume in IFNAR1-deficient mice (6). Indeed, murine models deficient in other elements of IFN signaling phenocopy the accelerated bone loss of the IFNAR1 and IFN-deficient mice (7). The mechanistic basis for how IFN-Is regulate osteoclastogenesis in turn derives from experiments in which IFNβ was noted to be induced acutely after initiation of osteoclastogenesis by RANKL (6). These

Author contributions: S.M., G.S., Y.A.-A., S.S., and E.M.G. designed research; S.M., P.K., S.C., C.M., G.S., Y.A.-A., and S.S. performed research; A.T. and K.A.F. contributed new reagents/analytic tools; S.M., P.K., A.T., C.M., G.S., Y.A.-A., S.S., and E.M.G. analyzed data; and S.M., P.K., A.T., S.C., C.M., K.A.F., S.S., and E.M.G. wrote the paper.

The authors declare no competing interest.

This article is a PNAS Direct Submission.

[1]To whom correspondence may be addressed. Email: Shruti.Sharma@tufts.edu or egravallese@bwh.harvard.edu.

This article contains supporting information online at https://www.pnas.org/lookup/suppl/doi:10.1073/pnas.2210409120/-/DCSupplemental.

Published April 6, 2023.

experiments have led to an understanding that IFN-I induction negatively regulates the process of RANKL-dependent osteoclastogenesis. However, IFNβ was found to be transiently induced very early (hours) after RANKL stimulation, whereas negative regulators are typically engaged much later in a cellular process, as is exemplified by the lag in autoregulation of NF-κB (8). Thus, we have explored additional IFN-I-dependent mechanisms that might also restrain osteoclastogenesis in vivo.

In homeostasis, IFN-I signaling is characterized by two main arms: 1) a "tonic" (also referred to as resting, "constitutive" or basal) arm, which serves to set baseline thresholds of critical immune response genes and 2) the better characterized, "inducible" arm, which is rapidly up-regulated in response to pathogenic insults (9). While the importance of inducible IFN-I is implicit in its well-described role in response to microbial infections, the requirement of constitutive IFN-I for immune homeostasis has proven harder to define (9). IFN-I signaling, through its receptor IFNAR, has a broad impact on key immune pathways through the greater than 700 downstream interferon-stimulated genes (ISGs) (10, 11). A thorough characterization of the transcriptional landscape as it pertains to both tonic and inducible ISGs was recently accomplished using IFNAR-deficient mice (11). Herein, inducible ISGs were defined as those whose expression was stimulated by IFNα, whereas tonic ISGs were defined as those that were decreased in otherwise unstimulated cells from IFNAR1-deficient mice (11). IFN-I-dependent suppression of osteoclast differentiation has been known for two decades, yet the mechanistic understanding of this signaling pathway, the expression of the tonic and inducible ISG groups, and the upstream factors shaping IFN-I signals in bone homeostasis have not emerged in the interim.

The stimulator of interferon genes (STING) pathway is one of the many pathways that induces IFNβ production, and STING is increasingly implicated as playing a pivotal role during infection and homeostasis (12–14). Aberrant STING activity has been tied to cancer, autoimmune and autoinflammatory diseases, including the disease STING-Associated Vasculopathy with onset in Infancy (SAVI), in which gain-of-function mutations in STING result in chronic inflammation, vasculopathy, and skin and pulmonary disease (14–17). STING-dependent innate immune responses have been best characterized in myeloid cells, which share a progenitor with osteoclast precursors (18). A role for STING in osteoclastogenesis has been suggested, but in the context of overt STING activation by one of its natural ligands, microbial derived cyclic dinucleotides (CDNs), or in the setting of ectopic overexpression of STING (19, 20). Not surprisingly, ligand-dependent STING activation is associated with induction of IFNβ and inhibition of osteoclastogenesis (19, 20) and mimics the treatment of osteoclast precursors with IFN-I. However, these previous studies linking STING activity and inhibition of osteoclastogenesis did not examine the role of endogenous STING in bone in vivo, nor did they investigate whether STING is routinely engaged in regulating osteoclastogenesis or the relationship of STING to IFN-I signaling in shaping osteoclast precursor fate.

Here, we tackle these outstanding questions and reveal the presence of tonic ISG expression in osteoclast precursors. In addition, we demonstrate a complex modulation of ISG expression by RANKL-RANK signaling in differentiating osteoclasts, clarifying the unique relationship of IFN-I with osteoclastogenesis. We identify STING as an immunomodulatory node regulating a unique and discrete tonic IFN-I signature in osteoclast precursors. Moreover, we identify ISG15 as a STING-dependent ISG that limits osteoclast formation. Our data suggest that STING signaling is a driver of intrinsic IFN-I signatures limiting osteoclast formation and that these osteoclast-intrinsic roles for STING signaling are critical in the homeostatic maintenance of bone in vivo. STING-deficient mice are shown to lose trabecular bone over time while, using conditional targeting, we demonstrate that myeloid-restricted STING signaling is sufficient to constrain osteoclastogenic potential and protect against bone loss in the setting of ovariectomy. Collectively, our data reveal STING as a previously unrecognized immunological "brake" on osteoclastogenesis in bone homeostasis and uncover unexplored avenues for therapeutic inquiry.

Results

Chronic Activation of STING Limits Osteoclast Differentiation through IFN-I Signaling. An understanding of how chronic activation of the STING pathway impacts osteoclast differentiation, in a clinically relevant setting, is absent. We turned to a murine model of chronic STING activation that results in disease (SAVI) to test its role in modulating osteoclast differentiation and function. Mice harboring the gain-of-function SAVI point mutation V154M (V155M in humans) recapitulate many aspects of the clinical features of SAVI and express an increased ISG profile (15). Osteoclast precursor cells from SAVI and WT mice were differentiated to mature osteoclasts in vitro. Fewer tartrate-resistant acid phosphatase-positive $(TRAP)^+$ multinucleated cells (MNCs) formed from SAVI osteoclast precursors in vitro compared to controls (WT) (Fig. 1*A*). $TRAP^+$ MNCs were quantified on day 4 after RANKL stimulation, revealing a statistically significant reduction in MNC formation in cells derived from SAVI bone marrow (Fig. 1*B*). Importantly, we find no difference in morphology or cell density in RANKL-naïve samples (d4 M-CSF only, *SI Appendix*, Fig. S1*A*) from SAVI or WT mice. SAVI cells exhibited a significant reduction in the expression of mRNA for several key markers of osteoclast differentiation, including cathepsin K (CTSK), calcitonin receptor (CalcR), and dendrocyte expressed seven transmembrane protein (DCSTAMP) (Fig. 1*C*).

A key outcome of STING activation in both chronic and acute settings is the mobilization of IFN-I signaling. SAVI osteoclast precursors produced increased CCL5 and CXCL10 in response to RANKL compared to WT-derived cells (*SI Appendix*, Fig. S1*B*), consistent with previous reports on ISG expression in SAVI mice (15). These increases were partially and significantly reduced by blocking IFNAR, as detected by reduced CCL5 and CXCL10 secretion at day 2 following RANKL stimulation. To evaluate whether STING-dependent IFN-I signaling is the principal mechanism for the inhibition of osteoclast differentiation in SAVI cells, an IFNAR1-blocking antibody or isotype control antibody was added to WT or SAVI osteoclast precursor cells in culture concurrent with RANKL stimulation. Addition of the anti-IFNAR1 antibody significantly increased the number of MNCs that formed from SAVI precursor cells compared to SAVI cells treated with isotype control antibody (Fig. 1*D*). To more thoroughly test the role of IFN-I in the inhibition of osteoclastogenesis in SAVI cells, osteoclast formation from littermate IFNAR KO and SAVI/IFNAR KO cells was tested. MNC formation was found to be no different in cells from the two genotypes, strengthening the link between STING activation and IFN-I in limiting osteoclastogenesis (Fig. 1*E*). These data extend prior studies in acute ligand-dependent activation of STING and demonstrate that chronic STING activity also inhibits osteoclast differentiation directly through the action of cell-intrinsic IFN-I.

STING Deficiency Accelerates Bone Loss over Time. Prior studies (19, 20) and the above data predict that STING activation may restrain osteoclast formation and serve as a key bone-protective mechanism in settings of inflammation and infection. However,

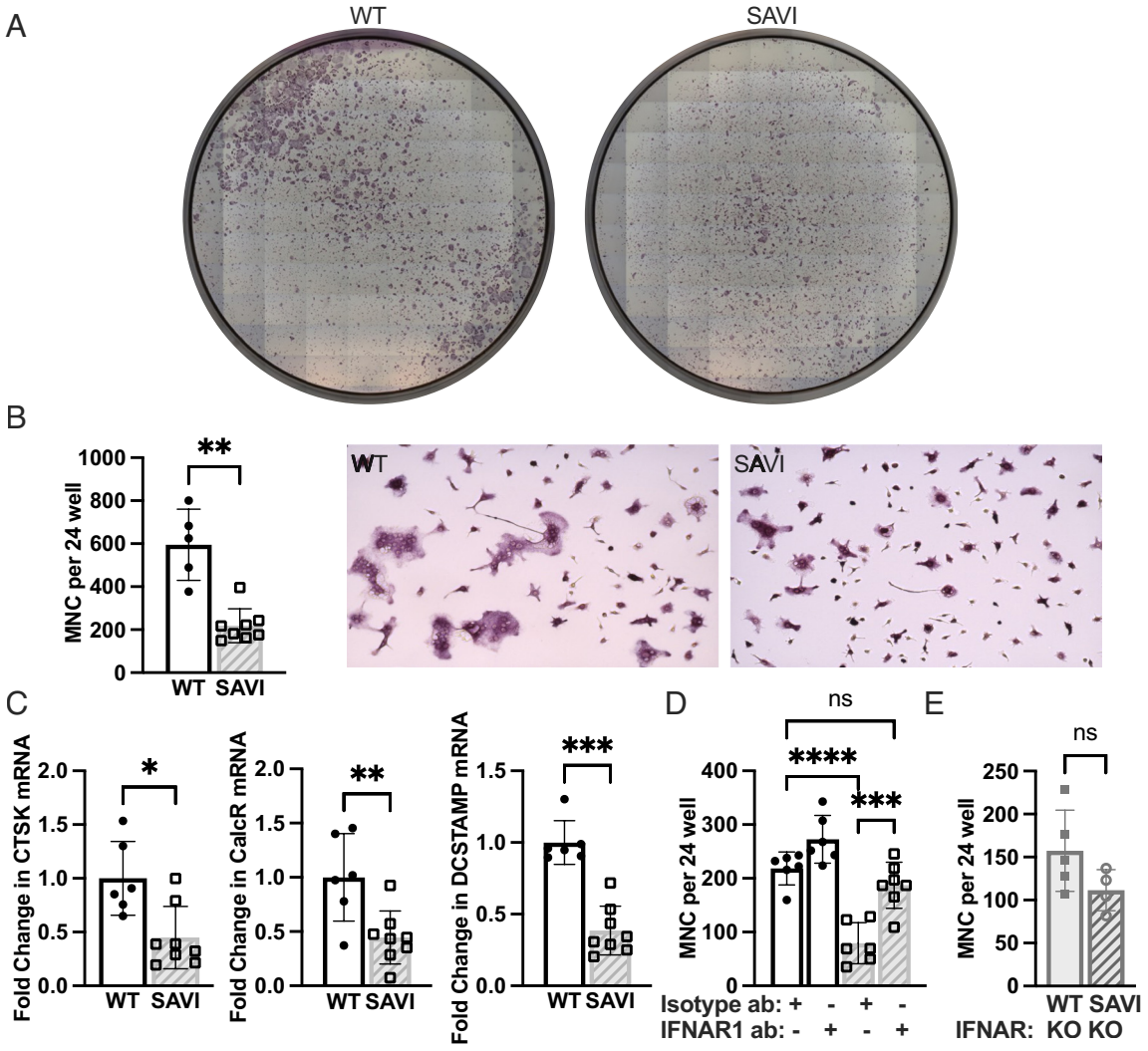

Fig. 1. Osteoclast precursors derived from SAVI mice exhibit reduced osteoclast formation in vitro, which is reversible with IFNAR1 blockade. (*A*) Representative stitched 10× images of tartrate-resistant acid phosphatase (TRAP)-stained cultures show fewer TRAP^{+} multinucleated cells (MNCs) in RANKL-stimulated SAVI osteoclast precursors compared to littermate WT precursors at day 5. (*B*) Quantification of MNCs at day 4 of RANKL stimulation shows fewer MNCs from SAVI mice (hatched bars) compared to littermate WT (clear bars). Representative images of TRAP-stained cultures are shown (20×; n = 5 WT and n = 8 SAVI). (*C*) qPCR of osteoclast differentiation genes in WT and SAVI cells at day 4 of RANKL stimulation shows that SAVI cells express less mRNA for key marker genes of osteoclast differentiation (CTSK, CalcR, and DCSTAMP) compared to WT (n = 6 WT and n = 8 SAVI). (*D*) Treatment of SAVI osteoclast precursors with anti-IFNAR1 antibody (IFNAR1 ab) significantly increases the number of MNCs formed compared to SAVI osteoclast precursors treated with isotype control at day 4 of RANKL treatment. SAVI cells form a similar number of MNCs in the setting of IFNAR1 blockade compared to WT cells treated with the isotype control (n = 6 to 7 per genotype). (*E*) Quantification of MNCs at day 4 post RANKL treatment shows no significant difference in the number of MNCs formed from SAVI/IFNAR KO mice (hatched bars) compared to IFNAR KO mice (clear gray bars). *P < 0.05, **P < 0.01, ***P < 0.001, ****P < 0.0001.

these studies do not address whether STING signaling plays a role in bone homeostasis in the absence of pathogenic stimuli. To determine a role for STING in bone homeostasis, bone parameters were assessed in STING-deficient aging mice. At 6 mo of age, male STING-deficient mice showed an increase in TRAP-expressing osteoclasts (Fig. 2 *A* and *B*) compared to controls (WT). The osteoclast surface per bone surface (Oc.S/BS) and number of osteoclasts per trabecular bone perimeter (Oc.N/B.Pm) significantly increased in STING-deficient mice compared to WT (Fig. 2*B*). Serum C-terminal telopeptide (CTX), a marker of osteoclast activity, increased in the 6-mo-old STING-deficient males compared to WT males (Fig. 2*C*). Trabecular bone analysis by microcomputed tomography (microCT) revealed a trend toward a reduction in trabecular bone volume/total bone volume (BV/TV) at 6 mo and 13 mo of age in STING-deficient males compared to WT controls (*SI Appendix*, Fig. S2 *A* and *B*). The trabecular network in the 13-mo-old STING-deficient mice exhibited a reduction in trabecular thickness (Tb.Th) (*SI Appendix*, Fig. S2*B*). By 15 mo of age, STING-deficient males exhibited a statistically significant decrease in trabecular BV/TV (Fig. 2 *D* and *E*), and a trabecular network characterized by increased trabecular spacing (Tb.Sp) and reduced trabecular number (Tb.N) (Fig. 2 *D* and *E*). 15-mo-old STING-deficient male mice also exhibited reduced trabecular bone volume (Tb.V) compared to WT, with no significant change in trabecular thickness (Tb.Th) (*SI Appendix*, Fig. S2*C*). This trabecular phenotype is evident in male STING-deficient mice but not in female STING-deficient mice (*SI Appendix*, Fig. S2*D*), suggesting that sexual dimorphism may shape the phenotypes of STING-deficient male and female mice. Hormonal changes influence a rapid bone loss in female mice starting at 6 mo of age and the subsequent loss of bone in female mice over time may override a role for STING in modulating bone volume (21).

Myeloid-Specific STING Suppresses Osteoclast Differentiation. Osteoclasts derive from the myeloid lineage (18). We thus generated myeloid-specific (STING^{Myl}) deficient mice to further determine the myeloid STING-specific contribution to bone loss. We performed bilateral or sham ovariectomies on STING^{Myl}-deficient

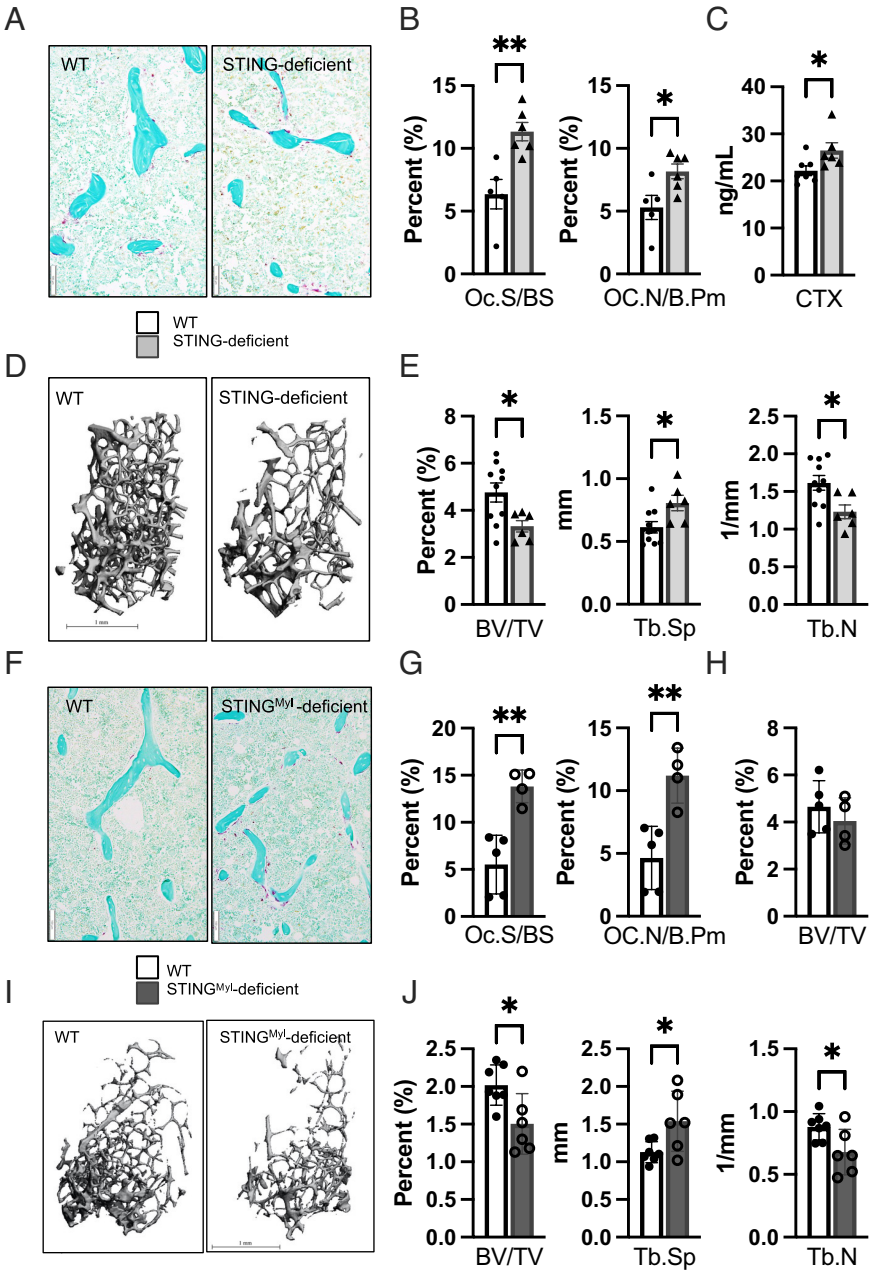

Fig. 2. STING-deficient mice show bone loss over time and post ovariectomy. (*A*) Representative TRAP-stained images (20×) in decalcified femurs from 6-mo-old male WT (*Left*) and STING-deficient (*Right*) littermates. (Scale bars indicate 100 μm.) (*B*) Quantification of percent osteoclast surface/bone surface (Oc.S/BS %) and osteoclast number/bone perimeter (Oc.N/B.Pm) in trabecular bone shows a significant increase in these parameters in the STING-deficient compared to WT mice (n = 5 WT and n = 6 STING-deficient). (*C*) CTX-I, a marker of osteoclast activity, is increased in serum from fasted 6-mo-old male STING-deficient mice compared to WT (n = 7 WT and n = 6 STING-deficient). (*D*) Representative reconstructed images of trabecular bone, distal femur, in 15-mo-old male WT and STING-deficient mice (Scale bar represents 1 mm). (*E*) Bone parameters in male STING-deficient and WT mice at 15 mo of age. Trabecular bone volume/total bone volume (BV/TV, %) in the distal femur is significantly reduced in STING deficiency. Trabecular spacing (Tb.Sp, mm) is significantly increased and trabecular number (Tb.N, 1/mm) is significantly decreased in 15-mo-old STING-deficient femurs (n = 10 WT and n = 6 STING-deficient). (*F*) Representative TRAP-stained images in decalcified femur 8 wk after sham surgery in WT (*Left*) and STING^{Myl}-deficient (*Right*) littermates. (Scale bars indicate 100 μm.) (*G*) Quantification of percent osteoclast surface/bone surface (Oc.S/BS %) and osteoclast number/bone perimeter (Oc.N/B.Pm) shows a significant increase in the osteoclasts per bone surface and per bone perimeter in STING^{Myl}-deficient mice compared to WT mice. (*H*) MicroCT analysis of trabecular bone, distal femur, shows no difference in trabecular bone volume in WT or STING^{Myl}-deficient mice after sham surgeries (n = 5 WT and n = 4 STING^{Myl}-deficient). No detectable difference was observed in trabecular bone (BV/TV, %) from WT and STING^{Myl}-deficient mice 8 wk following sham surgery. (*I* and *J*) Ovariectomies performed on female WT and STING^{Myl}-deficient littermates at 8 wk of age: STING^{Myl}-deficient mice exhibited enhanced trabecular bone loss (BV/TV, %) compared to WT mice. Trabecular parameters show increased trabecular spacing (Tb.Sp) and decreased trabecular number (Tb.N) (n = 7 WT and n = 6 STING^{Myl} deficient). * denotes $P < 0.05$; ** denotes $P < 0.01$.

and WT female mice to ascertain the impact of sexual dimorphism in the setting of myeloid STING deficiency. Similar to findings in global STING-deficient mice, more osteoclasts were observed on the surface of trabecular bone in STING^{Myl}-deficient mice 8 wk after sham surgery (Fig. 2 *F* and *G*). BV/TV did not differ between WT and STING^{Myl}-deficient mice 8 wk after sham surgery compared to WT sham controls (Fig. 2*H*); however, BV/TV was significantly reduced in STING^{Myl}-deficient mice 8 wk following OVX surgery compared to WT OVX controls (Fig. 2 *I* and *J*), accompanied by a statistically significant increase in trabecular spacing and reduction in trabecular number (Fig. 2*J*). There was also a significant reduction in the trabecular volume (Tb.V.) but not trabecular thickness (Tb.Th) 8 wk following OVX surgery in STING^{Myl}-deficient mice compared to WT OVX controls (*SI Appendix*, Fig. S2*E*). These in vivo studies indicate that STING deficiency increases osteoclast numbers, with a resultant bone loss phenotype over time, and support a role for myeloid STING in limiting osteoclast formation, even in the setting of rapid bone loss post ovariectomy.

STING Deficiency Promotes Osteoclastogenesis. To better define how STING regulates osteoclast numbers, M-CSF-expanded osteoclast precursors from STING-deficient and WT mice were treated with RANKL to induce TRAP^{+} multinuclear osteoclasts (MNCs). Significantly more MNCs formed from STING-deficient osteoclast precursors compared to WT osteoclast precursors. This effect was observed in osteoclast precursors from young mice (8 wk, Fig. 3*A*) and from 6-mo-old mice (Fig. 3*B*). We found no sex-based differences in the rate of formation of osteoclasts in vitro, and these data are pooled from male and female mice. Strengthening the role of myeloid STING in selectively inhibiting osteoclast formation, in vitro osteoclastogenesis assays using osteoclast precursors from STING^{Myl}-deficient male and female mice (8 wk) also formed significantly more osteoclasts than cells from WT mice (Fig. 3*C*). Supporting an inhibitory role for STING in osteoclastogenesis, STING mRNA and protein expression levels both decrease during RANKL-stimulated osteoclastogenesis in WT cells (Fig. 3*D*).

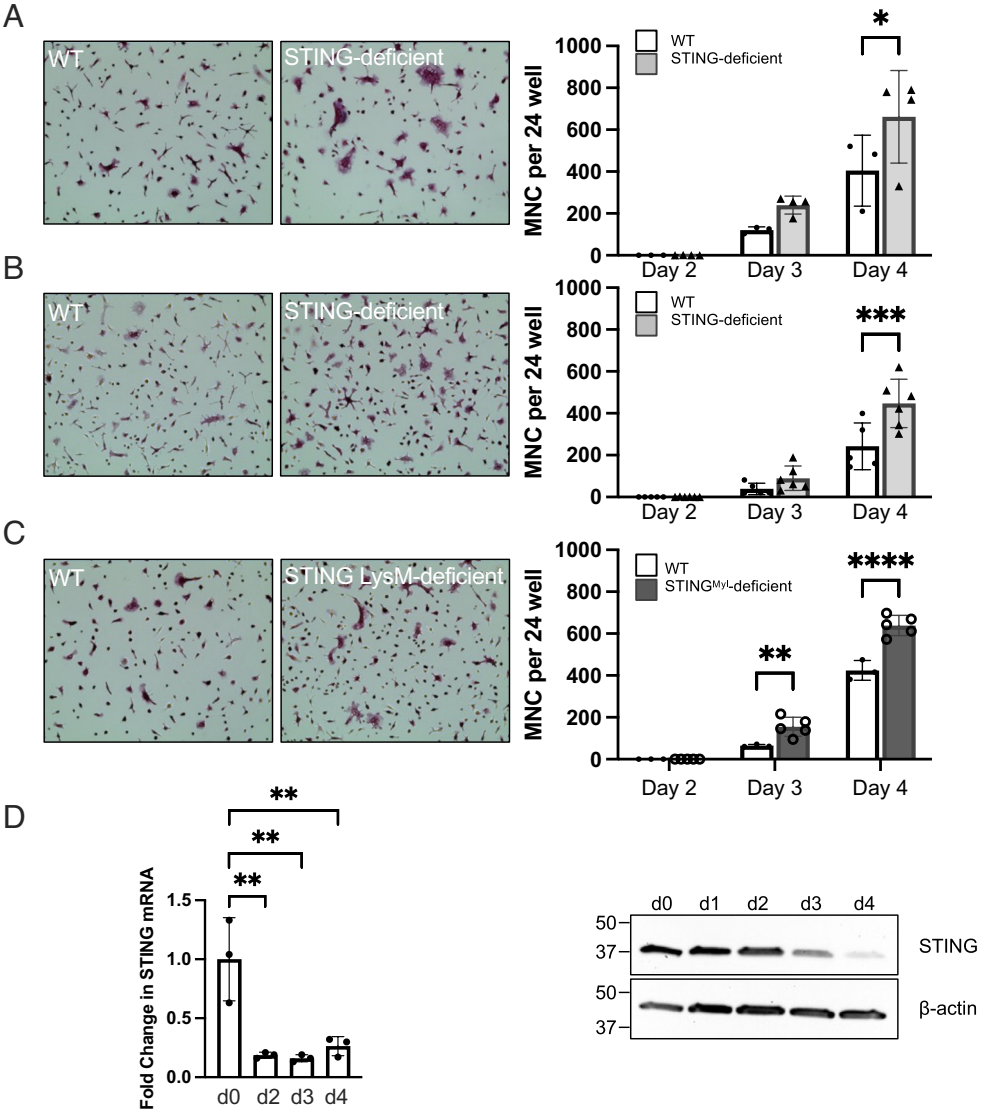

Fig. 3. STING deficiency promotes osteoclast differentiation. (*A*) Primary osteoclast precursors from 8-wk-old STING-deficient mice and littermate wildtype (WT) controls were M-CSF expanded and induced to form osteoclasts in vitro following addition of RANKL on day 0. Quantification of $TRAP^+$ multinuclear cells (MNCs) revealed that STING-deficient osteoclast precursors formed more osteoclasts (n = 3 WT and n = 4 STING deficient). Representative 20× images from WT and STING-deficient cultures after RANKL stimulation, d4, are shown to the left for all conditions. (*B*) Osteoclast precursors from 6-mo-old STING-deficient and littermate WT mice were induced to form osteoclasts following addition of RANKL. More MNCs formed from older STING-deficient osteoclast precursors compared to older WTs (n = 5 WT and n = 6 STING deficient). (*C*) Osteoclast precursors from 8-wk-old $STING^{Myl}$-deficient mice formed more MNCs under differentiation conditions compared to littermate WTs (n = 3 WT and n = 5 $STING^{Myl}$ deficient). (*D*) qPCR analysis (*Left*) and western blot (*Right*) from differentiating osteoclasts showed that STING mRNA and protein are expressed in unstimulated cells and expression decreased during osteoclast differentiation. *$P < 0.05$; **$P < 0.01$, ***$P < 0.001$, ****$P < 0.0001$.

STING Signaling Shapes a Core Tonic ISG Cassette Lost during RANKL-Induced Osteoclastogenesis. To comprehensively evaluate the impact of STING expression and signaling on osteoclast formation, we carried out unbiased RNA sequencing on osteoclast precursors (RANKL naïve, d0) and RANKL-stimulated, differentiating osteoclasts at days 2, 3, and 4 from both WT and STING-deficient mice (Fig. 4*A*). A pairwise comparison of all experimental groups revealed 10,721 differentially expressed genes during osteoclast differentiation (*SI Appendix*, Fig. S3*A*). Key genes were validated by quantitative PCR in an independent set of RNA from WT and STING-deficient osteoclast precursors, emphasizing the robustness of the dataset (*SI Appendix*, Fig. S3*B*). Analysis of differentially expressed genes at varying stringency levels revealed that 337 genes could define the significant differences between the WT and STING-deficient cells ($P \leq 0.05$). However, the most significantly different genes ($P \leq 0.01$) are represented in a codeset of 90 differentially expressed genes and can effectively separate WT and STING-deficient osteoclast precursors and differentiating cells independent of timepoint (d0, 2, 3 and 4). A heatmap representation of the 90 gene set reveals how expression patterns of these key genes distinguish WT and STING-deficient cells (Fig. 4*B*). A comparison with published datasets of ISGs (11) identified 27 ISGs (marked by asterisks) in this 90 gene codeset that were further found to be significantly altered in STING-deficient cells (Fig. 4 *B*, *Inset*).

Unexpectedly, many of the genes discriminating WT from STING-deficient cells were expressed at day 0, prior to the addition of RANKL. An unsupervised PCA of sample distribution based on the 90-gene expression analysis reveals that the biggest differences are indeed notable at day 0, i.e., in RANKL-naïve osteoclast precursors (Fig. 4*C*). Reactome-based enrichment analysis of this 90-gene codeset confirmed IFN-I signaling as the predominant pathway impacted in differentiating STING-deficient osteoclast precursors (Fig. 4*D*). The most highly enriched pathway

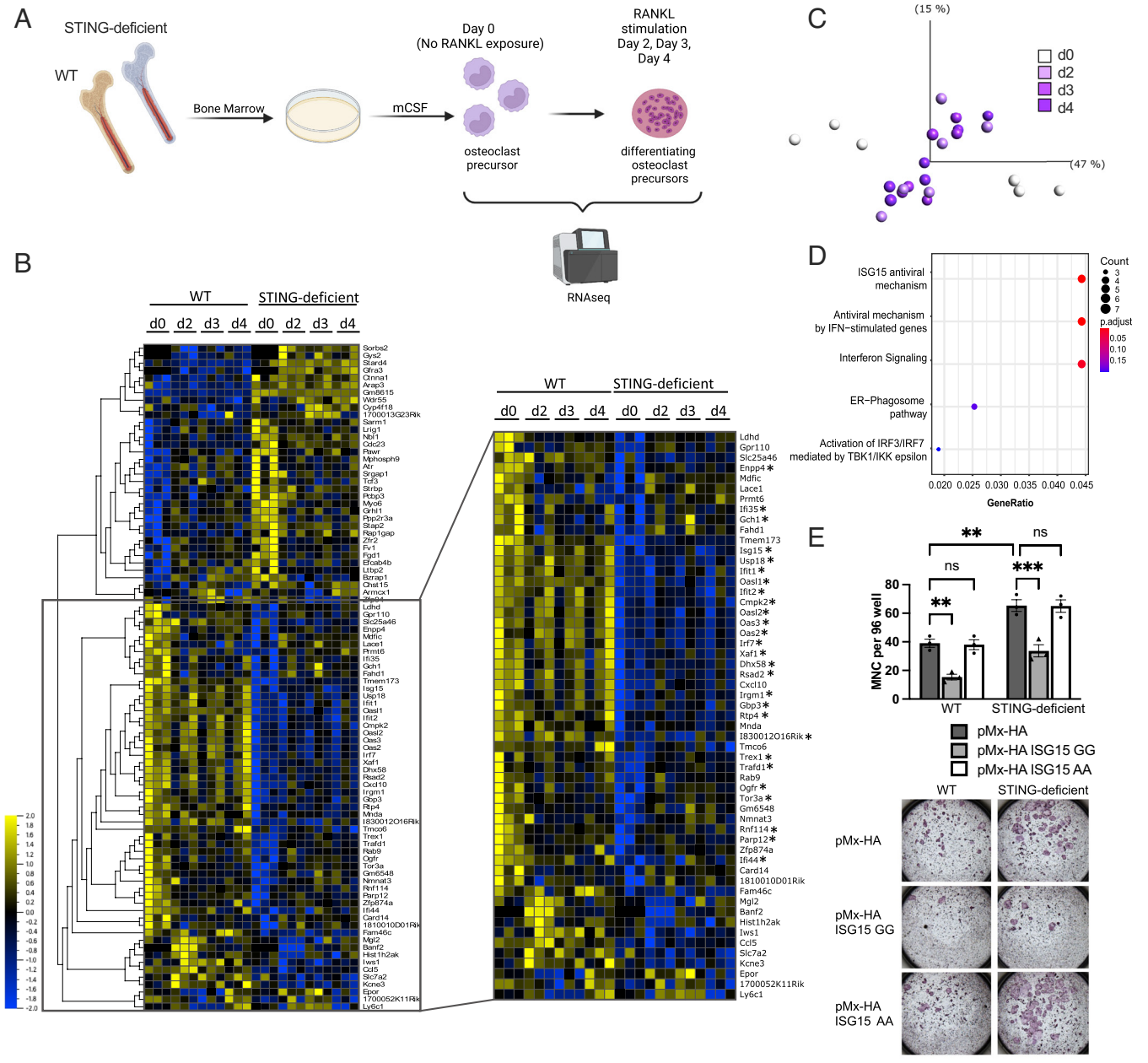

Fig. 4. Global transcriptomics reveal a STING-dependent IFN-I signature in osteoclast precursor cells. (*A*) Schematic representation of sample preparation for RNA sequencing. Samples from littermate WT and STING-deficient M-CSF-expanded bone marrow cells (day 0, d0) and following RANKL stimulation (d2, d3, and d4) were analyzed by pairwise comparisons (n = 3 WT and n = 3 STING deficient at each timepoint). Panel *A* was created with Biorender.com. (*B*) Time nominal heatmap analysis of gene expression in WT and STING-deficient osteoclasts (d0-d4), highlighted 90 differentially expressed genes between the experimental groups. The box emphasizes the expression pattern of primarily ISGs that are significantly down-regulated in STING-deficient cells. Scale represents range in row means. * denotes a previously described macrophage ISGs as defined in ref. 11. (*C*) PCA of the 90 differentially expressed genes defined in *B* underscores that the most disparate experimental groups are the WT and STING-deficient RANKL-naïve cells (d0). (*D*) Unbiased Reactome-based gene set enrichment analysis of the 90 genes in *B* reveals significant enrichment of genes in IFN-I pathways that are expressed in a STING-dependent manner. All analyses were delimited by a T of 0.01 and $P \leq 0.01$, unless noted otherwise. (*E*) WT and STING-deficient bone marrow macrophages were infected with pMx-HA-ISG15GG (WT) or pMx-HA-ISG15AA (mutant). Cells were then plated in 96-well plates in the presence of RANKL (50 ng/mL) and M-CSF (10 ng/mL) for 4 d, followed by TRAP staining. The MNCs per well were enumerated and represent an average of three independent replicates. $^{**}P < 0.01$, $^{***}P < 0.001$, ns = not significant. Two-way ANOVA.

identified was "ISG15 antiviral mechanism." ISG15-deficient osteoclast precursor cells were previously shown to have enhanced osteoclast formation in RANKL-induced differentiation assays compared to WT (22, 23), similar to our findings with STING-deficient osteoclast precursors. To test the direct contribution of ISG15 downstream of STING during osteoclastogenesis, WT and STING-deficient osteoclast precursor cells were transduced with either native ISG15 (ISG15GG) or an ISGylation-incompetent form of ISG15 (ISG15AA). Indeed, expression of the active ISG15, but not the inactive form, limited osteoclast formation in both WT cells and STING-deficient cells. (Fig. 4*E*). These data provide a mechanistic link between STING and ISG15 in the inhibition of osteoclastogenesis.

The expression of ISGs at day 0, prior to the addition of RANKL, was reminiscent of previously described tonic IFN-I signatures (11). The sources of tonic IFN-I in many cell types remain unknown but based on these observations, we hypothesized that STING plays a role in regulating tonic ISG expression in osteoclast precursors at day 0 and in differentiating osteoclast precursors. While the expression of IFNβ and a handful of ISGs has been

shown to be increased shortly after RANKL stimulation (6), no studies have systematically mapped the tonic and inducible ISG landscape during osteoclast formation. In order to evaluate the contribution of STING-dependent ISGs in osteoclast precursors and differentiating osteoclasts, we first needed to establish the dynamics of ISGs in toto in WT osteoclast precursors and differentiating cells. Using previously published datasets, we generated a list of 720 ISGs identified by RNA sequencing in immune cells (11). These 720 ISGs were categorized either as inducible (those increased with IFNα treatment) or tonic (those decreased in unmanipulated IFNAR1-deficient cells) (11). Of these 720 ISGs, 638 were identifiable in our dataset. Intriguingly, we note significant heterogeneity in the expression patterns of the 638 ISGs during osteoclastogenesis and describe three broadly segregable ISG clusters. Consistent with, but expanding upon, the well-established observation that RANKL stimulates IFN-I production, we identified a cluster of RANKL-*induced* ISGs (Fig. 5*A*). A separate cluster of RANKL-*repressed* ISGs was also identified (Fig. 5*B*). The RANKL-repressed gene set represents a previously unappreciated role for RANKL in inhibiting ISGs and suggests that this subset of ISGs may play an inhibitory role, restraining osteoclast precursors from osteoclastogenesis. A third cluster of genes with a variable response to RANKL was also identified (*SI Appendix*, Fig. S3*C*) and represents ISGs with mixed characteristics, indicating a complex role for IFN-I in osteoclastogenesis.

To further define these clusters, we queried the overlap of each cluster with previously defined tonic ISGs. The greatest overlap was noted between the RANKL-repressed genes and tonic ISGs, with nearly one-third of the ISGs falling within RANKL-repressed ISG cluster (90 of 306) identified as tonic. Only 19 of the 235 RANKL-induced ISGs were tonic ISGs, and of the 97 mixed RANKL-response ISGs, only 14 were tonic ISGs (Fig. 5 *A* and *B* and *SI Appendix*, Fig. S3*C*). Therefore, these data uncover a large subset of ISGs that are repressed by RANKL compared to the RANKL-naïve precursor cells and highlight that a large number of the RANKL-repressed ISGs are comprised of previously defined tonic ISGs.

To characterize the contribution of STING in shaping this basally expressed tonic ISG signature, we determined that WT and STING-deficient osteoclast precursors (d0) can be effectively separated by the expression of a 234-gene cassette that includes both up- and down-regulated genes in STING-deficient cells (*SI Appendix*, Fig. S3*D*). Of these 234 genes, many are ISGs. However, only 50 genes overlap with RANKL-repressed ISGs and are significantly down-regulated in the STING-deficient osteoclast precursor cells compared to the WT (Fig. 5*D*). This 50 gene set can be categorized as a STING-dependent ISG subset, which includes ISG15. The expression pattern of these 50 ISGs closely mirrors the downregulation of STING expression itself, suggesting that they are expressed in a tonic capacity in the presence of STING and are actively down-regulated by RANKL during osteoclastogenesis.

Intriguingly, many of the STING-regulated tonic ISG genes are also up-regulated in SAVI V154M and are dependent upon IFNAR expression, including *Il-18*, *Irf7, Zbp1, Ifi47, Cxcl10*, *Ifit2*, *Rsad2 (Viperin)*, and *Ifit1* (15). Together, these data indicate that this core ISG signature (50 ISGs) is specifically modulated by STING activity in settings of chronic activation (SAVI) and during normal osteoclastogenesis, when STING expression itself is downmodulated. Upstream regulators of a tonic IFN-I signature are poorly defined during osteoclastogenesis. Our data elucidate that STING is a modulator of tonic ISG signaling, with a specific signature of ISGs that is correlated with its own expression. Critically, we reveal that this regulation of ISGs via STING provides a brake for osteoclastogenesis and plays a role in shaping the ability of osteoclast precursors to commit to becoming mature osteoclasts, thereby regulating bone mass.

Discussion

IFN-I signaling as a mechanism of RANKL-stimulated autoinhibition of osteoclastogenesis has been a foundational basis for how IFN-Is contribute to bone homeostasis. Here, we reveal an unexpected contribution of IFN-I-stimulated gene expression as a tonic regulator of osteoclastogenesis. We identify the innate immune adaptor STING as a regulator of bone homeostasis and demonstrate that the STING pathway provides protection from in vivo bone loss over time. Several unique features of STING-dependent signaling in the regulation of bone are uncovered by our findings, including its cell-intrinsic function and its role in establishing a tonic ISG signature in osteoclast precursor cells. STING-deficient osteoclast precursor cells differentiate more efficiently than WT cells to osteoclasts, consistent with the concept that STING signaling inhibits osteoclastogenesis. Finally, we identify patterns of tonic and inducible ISG expression in osteoclast precursors and maturing osteoclasts, emphasizing a dynamic relationship of IFN-I signatures with osteoclastogenesis. A schematic of our proposed model for the role of STING-dependent IFN-I and ISGs in the inhibition of osteoclastogenesis is outlined in Fig. 6.

Tonic or constitutive IFN-I signaling is an often underappreciated aspect of IFN-I signaling that has been proposed to be a critical element of homeostasis. Vital for maintaining a balanced threshold of immune genes, tonic IFN-I signatures serve either to augment or suppress diverse cytokine responses activated during an immune response (9, 11). Tonic ISGs are defined as the network of ISGs that are decreased in IFNAR1-deficient compared to WT mice in the absence of a pathogenic stimulus (11). Intriguingly, in the process of osteoclastogenesis, the original studies by Takayanagi et al. focused predominantly on RANKL-induced IFN-I production (6). However, they also describe a baseline expression of IFNb in RANKL-naïve osteoclast precursor cells, indicating active tonic IFN-I signaling prior to RANKL stimulation (6). The contributions of tonic IFN-I signaling were not considered central to osteoclastogenesis and were neither identified as tonic IFN-I nor further characterized in the field. Further studies also focused on the inhibitory action of RANKL-induced ISGs on osteoclastogenesis (24) or provided evidence for the impact of tonic ISGs on osteoblast formation (25, 26). Given these findings, a systematic understanding of tonic IFN-I in osteoclasts is warranted.

Here, we leverage an unbiased gene expression analysis of RANKL-naïve and RANKL-stimulated osteoclast precursors. We reveal unexpected patterns of IFN-I signaling during the different stages of osteoclastogenesis. Consistent with Takayanagi's findings, a large set of ISGs were determined to be up-regulated in a sustained (occurring over days) fashion by RANKL (RANKL induced; 235 genes). However, a minority of these genes (19 genes) are identified as tonic ISGs (11). An important observation is the identification of a prevalent, tonic IFN-I signature in RANKL-naïve cells (day 0). Intriguingly, this large cluster of tonic ISGs that are expressed at day 0 in WT cells are repressed in the presence of RANKL (RANKL repressed; 306 ISGs), indicating that this baseline ISG signature in osteoclast precursors may shape their readiness for terminal differentiation. The robust downregulation of ISGs upon the commitment of precursors to osteoclastogenesis after RANKL exposure is the clearest support for how, as negative regulators of osteoclastogenesis, key ISGs must be rapidly down-regulated before osteoclastogenesis can proceed. These findings then suggest that basal or tonic ISG signatures serve as "brakes" on osteoclastogenesis, and their restraint on

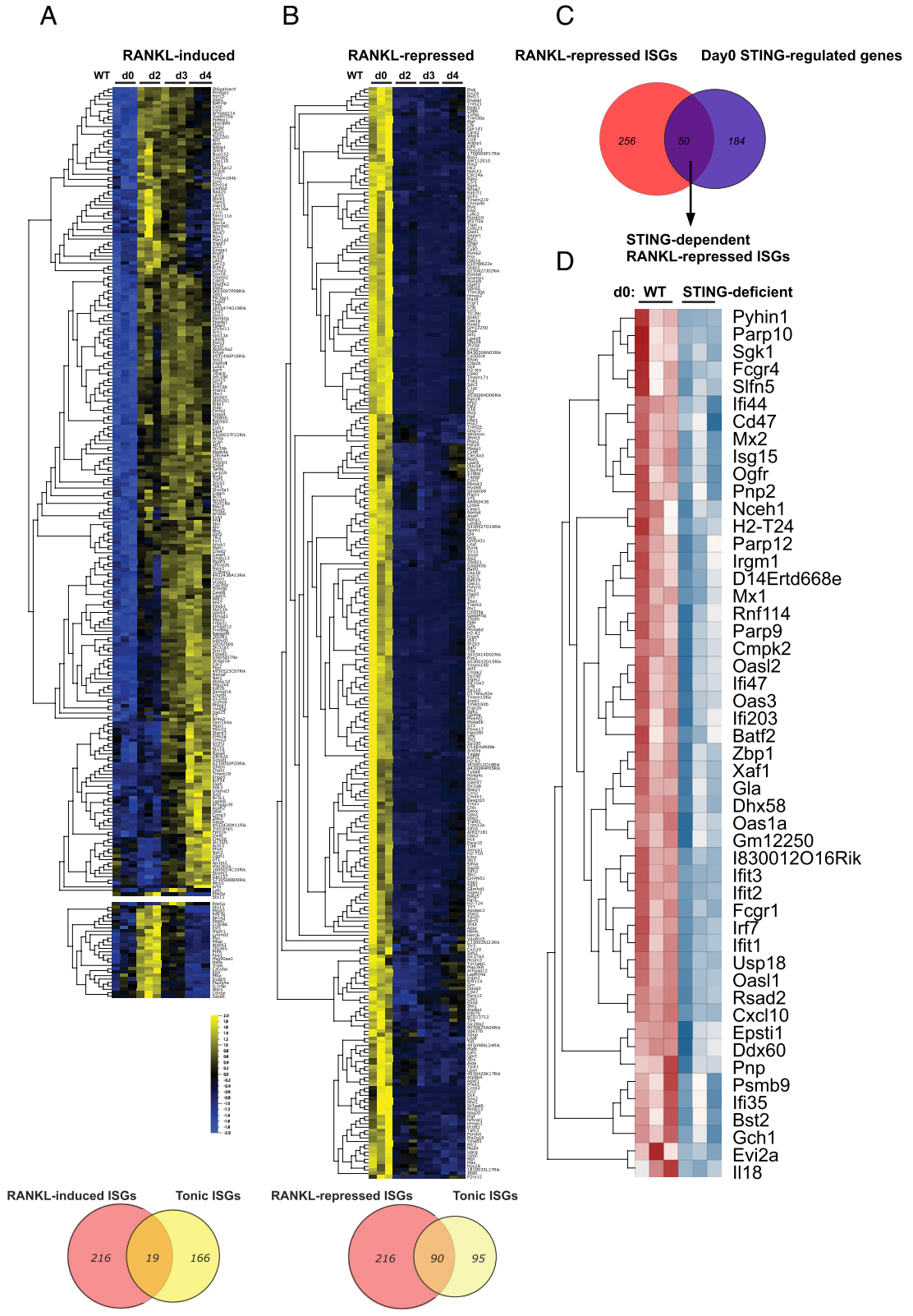

Fig. 5. Osteoclast precursor transcriptomes possess a STING-dependent tonic IFN-I signature. Targeted gene expression analysis in WT osteoclast precursors or differentiating osteoclasts reveals two main subsets of ISGs which are significantly altered during differentiation ($P \leq 0.01$). (*A*) RANKL induced and (*B*) RANKL repressed. Overlap of these ISGs subsets with previously described tonic ISGs is shown in the Venn diagrams below each heatmap. (*C*) Venn diagram representation of the overlap between RANKL-repressed genes from *B* and genes altered at day 0 (d0) in STING-deficient osteoclast precursors identify a cassette of 50 STING-dependent RANKL-repressed ISGs. (*D*) Heatmap expression analysis of this 50 gene codeset in RANKL-naïve WT and STING-deficient osteoclast precursors (d0).

differentiation exists in osteoclast precursor cells before they experience RANKL.

A comparison of RNAseq datasets from STING-deficient and WT osteoclast precursor cells (day 0, RANKL naïve) highlights the overrepresentation of IFN-I pathways in WT cells that are lost in STING-deficient cells at this timepoint. This, then, provides a compelling argument for STING-dependent regulation of tonic IFN-I signaling in osteoclast precursors. Indeed, we identify a

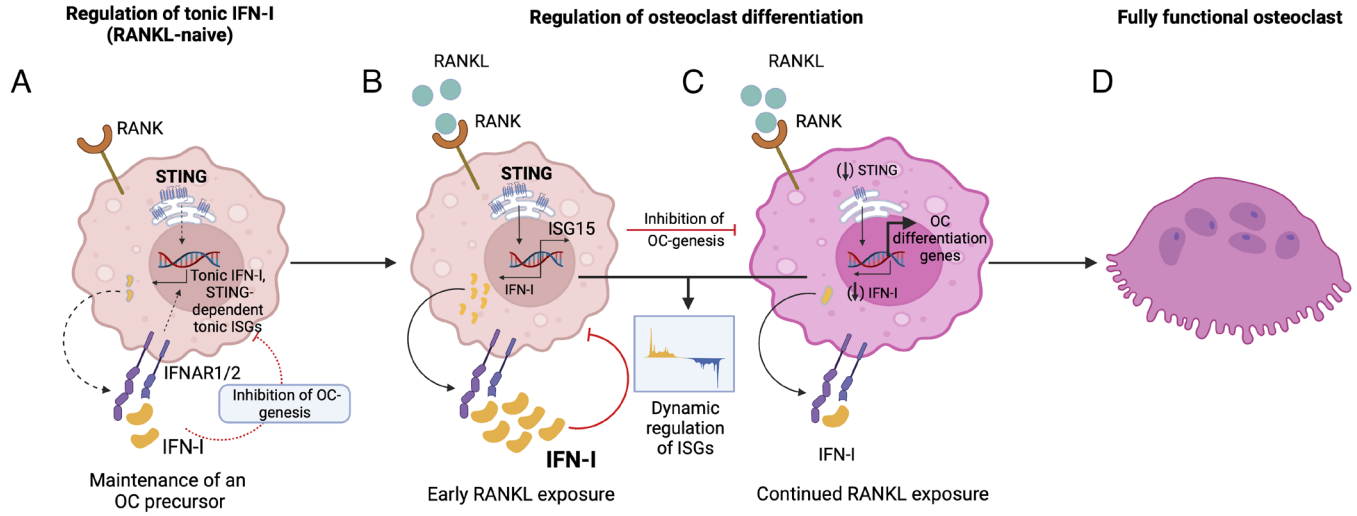

Fig. 6. Proposed model for STING-dependent regulation of osteoclastogenesis. (*A*) Regulation of IFN-I: RANKL-naïve osteoclast precursors (OC precursors) rely on STING-dependent tonic IFN-I and downstream ISG expression, such as ISG15 and potentially others, to provide a brake on osteoclastogenesis (OC-genesis). Dotted black lines denote tonic (baseline) signaling downstream of STING. Dotted red line denotes inhibition of OC-genesis. Regulation of osteoclast differentiation: (*B*) Early RANKL exposure drives induction of IFN-I and dynamically regulates multiple ISGs, at least in part through STING activation. STING-dependent upregulation of ISG15 further limits OC differentiation. Red lines denote inhibition of OC-genesis. (*C*) Continued RANKL exposure down-regulates the expression of STING, IFN-I, and ISGs, promoting the program of expression of OC differentiation genes, resulting in the differentiation of OC precursor cells to fully functional OCs (*D*). Figure was created with Biorender.com.

contingent of 50 ISGs that are STING dependent in RANKL-naïve precursors. Importantly, we find that the majority (40 genes) of the STING-regulated 50 ISG subset are previously described tonic ISGs. The remaining 10 ISGs are apparent osteoclast precursor specific, STING-dependent, tonic ISGs. Collectively, these data demonstrate an intrinsic and specific role for STING-dependent signaling in specifying a tonic ISG signature that shapes the fate of osteoclast precursor cells.

We performed an extensive literature review on the ISGs included in our STING-dependent, tonic IFN signature with regard to their role in osteoclastogenesis and bone. This list revealed multiple genes with known proosteoclastogenic role [CXCL10 (27, 28), IL18 (29)], an antiosteoclastogenic role [USP18 (30), RNF114 (31)], and others which have no previous links to bone homeostasis. This review in conjunction with identification of ISG15 antiviral mechanism as the most significant pathway from our Reactome analysis suggested that dysregulation of ISG15 may contribute to the STING-deficient bone phenotype. ISG15 is a ubiquitin-like protein that is covalently added to proteins through the process of ISGylation. ISGylation requires the C-terminal glycine–glycine (GG) sequence of ISG15 to tag targeted proteins (32). ISG15 has complex roles in the regulation of cell function as protein ISGylation can promote either the degradation or stability of the target protein. In addition to ISGylation, soluble ISG15 can have ISGylation-independent roles (Reviewed in ref. 33). Previous studies identified that deficiency of ISG15 promotes osteoclastogenesis, phenocopying STING deficiency in differentiating osteoclast precursor cells (22). By RNA sequencing, we validate that ISG15 is down-regulated in RANKL-naïve osteoclast precursors from STING-deficient mice compared to WT controls.

Given ISG15's tonic regulation by STING and its previously described role in osteoclastogenesis, we sought to determine whether ISG15 plays a role in STING-dependent regulation of osteoclastogenesis. In STING-deficient osteoclast precursor cells, ectopic expression of wild-type ISG15 (ISG15GG), but not the ISGylation-inactive form (ISG15AA), decreases osteoclast formation. Indeed, STING-deficient +ISG15GG osteoclast precursors differentiate at a rate similar to WT osteoclast precursors. This observation supports the hypothesis that STING-dependent regulation of ISG15 expression limits osteoclastogenesis and provides a link between STING and ISGylation. Thus, ISG15 is a key STING-dependent ISG that limits osteoclastogenesis. The complexity of other known regulators of osteoclastogenesis in our 50 ISG subset suggests that further research is required to understand the potential roles and interactions of these ISGs.

Consistent with our proposed role for STING signaling in determining the fate of osteoclast precursors, STING-deficient osteoclast precursor cells exhibit enhanced differentiation in response to RANKL stimulation. These data elucidate a link between the STING-dependent tonic ISG signatures in precursor cells and downstream osteoclastogenesis. Intriguingly, the expression of STING itself (mRNA and protein) is down-regulated in osteoclast precursors as they differentiate to osteoclasts. Collectively, these data suggest that a critical thrust of STING activity is in specifying gene expression before RANKL exposure, within osteoclast precursors. While the bulk of ISGs are expressed in RANKL-naïve osteoclast precursors at d0, a distinct set of ISGs is expressed at different times after RANKL exposure during osteoclastogenesis ("RANKL mixed-response genes"), as revealed by our comprehensive transcriptomic analysis. These findings reorient our basic understanding of how IFN-I signaling shapes the entirety of the osteoclastogenesis process, from lineage commitment of a precursor to the ligand-dependent maturation of osteoclast precursor cells into terminally differentiated osteoclasts. Our findings reveal that ISGs have a multifaceted role as regulators of osteoclastogenesis.

Importantly, the in vitro differences in osteoclastogenesis in STING-deficient and control cells are reflected in vivo, with increased numbers of osteoclasts in STING-deficient mice. Furthermore, STING-deficient male mice, in the absence of disease, develop reduced trabecular bone mass over time. These data provide experimental proof for a physiological role of STING in bone homeostasis. The overall rapid bone loss seen with age in female mice likely obscures a role for STING in this setting. This conclusion is consistent with the observation that no differences are notable in the differentiation kinetics of osteoclast precursors from male or female mice. To better understand the phenotypic

sex differences in bone as mice age, we performed ovariectomies in young STING^{Myl}-deficient mice to accelerate bone loss. STING^{Myl}-deficient female mice exhibit accelerated bone loss following ovariectomy, strengthening the observation that there is a STING-dependent inhibition of osteoclastogenesis, which may be obscured by age and hormone-associated acceleration of bone loss in females. Importantly, we also demonstrate that STING deficiency in myeloid precursors of osteoclasts is sufficient to recapitulate increased osteoclastogenesis in vitro and reveal that STING-dependent regulation of bone homeostasis is a myeloid intrinsic phenomenon.

In a prior study, we described a very different role for STING in promoting a bone accrual phenotype (34). This was in a setting of cytosolic DNA accrual and IFNAR deficiency. In this mouse model, deficiency in DNase II led to an abundance of intracellular DNA, which can activate multiple pattern recognition receptors including the STING pathway. DNase II deficiency is embryonically lethal but can be rescued by IFNAR deficiency (35–37). In the setting of DNase II and IFNAR double deficiency, mice develop inflammatory polyarthritis and other manifestations of autoimmunity, as well as accrual of trabecular bone in long bones that is IFN independent. The role of IFN-I downstream of STING could not be assessed in this context (34). We observed that deleting STING in DNase II/IFNAR double-deficient mice results in a reversal of this long-bone accrual. However, certain aspects of the autoimmune phenotype in these mice were also reversed in the setting of STING deficiency, including abrogation of the prominent inflammatory polyarthritis. Therefore, in this unique setting, STING may not be directly orchestrating trabecular bone formation but rather regulating the expression of an additional factor or factors that may promote bone formation.

A recent explosion in the understanding of STING signaling has underscored the importance of this ubiquitous pathway in a variety of disease states. Gain-of-function mutations in STING, which cause constitutive activation of STING signaling (15), have recently been described as drivers of the pediatric autoinflammatory disease SAVI (15, 16). We show that chronic signaling from the SAVI (STING V154M) allele in osteoclast precursors powerfully suppresses the differentiation of osteoclast precursor cells to osteoclasts. Importantly, SAVI osteoclast precursors fail to up-regulate key osteoclast differentiation genes with RANKL treatment that are known to be inhibited by IFN-I (6). These data support previous publications showing that STING activity limits osteoclast differentiation (19, 20). Our data also show that a blockade of IFN-I signaling or IFNAR-deficiency rescues the inhibition of osteoclast formation seen in SAVI osteoclast precursors, indicating that these low levels of IFN-I signaling are sufficient to shape osteoclast differentiation. These findings provide direct evidence that STING limits osteoclast differentiation by modifying IFN-I signaling. We have also compared the 50 STING-dependent tonic ISGs to a previously published dataset of 100 ISGs in SAVI V154M bone marrow-derived macrophages (15). Many of the STING-regulated tonic ISG genes have been shown to be up-regulated in SAVI V154M and are dependent upon IFNAR expression, including *Il-18, Irf7, Zbp1, Ifi47, Cxcl10, Ifit2, Rsad2 (Viperin),* and *Ifit1* (15), indicating that tonic STING signaling is dysregulated in the SAVI setting and may contribute to the inhibition of osteoclastogenesis in SAVI cells.

An unresolved question is how STING signaling is initiated in a constitutive or inducible manner during osteoclastogenesis. This fundamental question forms the basis of future studies but is also an open line of inquiry in other immune cell types in the field. Various endogenous ligands, including mitochondrial DNA, micronuclei, endogenous retroelements, nucleic acids from dying cells, or microbiome-derived cyclic di-nucleotides (14), are candidates. In addition, ligand-independent models for STING activation in macrophages have been proposed (38) but are not yet implicated in settings where tonic ISG signatures are noted.

In conclusion, our study uncovers a mechanistic link between STING signaling and IFN-I-dependent suppression of osteoclastogenesis. We strengthen this finding by showing a significant role for STING signaling in shaping tonic ISG signatures in osteoclasts and their precursors and in bone homeostasis in vivo. These observations contribute to our conceptualization of STING signaling as providing a physiological brake on osteoclastogenesis. With the advent of agonists and antagonists of the STING pathway that can be used therapeutically, the identification of a STING-dependent regulatory node in osteoclastogenesis reveals unexplored therapeutic avenues for osteopenic disorders and age-associated osteoporosis.

Materials and Methods

Mice. Whole-body STING-deficient mice were kindly provided by Glen Barber (39) and wild-type (WT) littermates were used as controls. STING$^{flox/flox}$ mice (Jackson Laboratories, 031670) (40) were bred to LysM-Cre mice (Jackson Laboratories, 004781) (41) to create homozygous STING$^{flox/flox}$; LysM-Cre$^{+/-}$ (designated as STING$^{Myeloid(Myl)}$ deficient) and STING$^{flox/flox}$;LysM-Cre$^{-/-}$ (with the latter designated as WT littermate controls). In vitro validation studies demonstrated that a single copy of LysM-Cre in a STING$^{flox/flox}$ mouse background reduced STING mRNA expression by more than 90% compared to WT (STING$^{flox/flox}$;LysM-Cre$^{-/-}$) (*SI Appendix*, Fig. S4). SAVI V154M heterozygous mice and littermate controls as well as SAVI V154M/IFNAR KOs and littermate IFNAR KOs were bred as previously described (15). All animal strains were maintained by heterozygous breeding leading to closed colonies. In all strains, the appropriate WTs were generated as a result of selective breeding. For all studies, WT indicates the appropriate littermate control for the indicated strain. Animal protocols were reviewed and approved by the Institutional Animal Care and Use Committees of the University of Massachusetts Chan Medical School, Washington University School of Medicine in St Louis, and the Brigham and Women's Hospital.

Serum Analysis. Mice were fed standard chow and kept on a 12 h:12 h light:dark cycle. At specified ages, mice were fasted for 16 h, sacrificed and serum was collected by terminal cardiac puncture. Serum from mice fasted for 16 h was analyzed for the C-telopeptide of collagen type I (RatLaps™ CTX-I, Immunodiagnostic Systems, AC-06F1) as a marker of bone catabolism.

Ovariectomy (OVX) Surgery. Eight- to nine-week-old WT and STING$^{Myeloid(Myl)}$-deficient female mice were anesthetized with isoflurane and bilateral ovariectomy was performed as previously described (42, 43). The mice were randomly assigned to sham or OVX surgery. Eight weeks after surgery, the mice were fasted for 16 h prior to euthanasia. Trabecular and cortical bone parameters were measured by microCT in the femur as described below.

Microcomputed Tomography (microCT). Femurs were fixed in 3.7% formaldehyde for 3 d and transferred to 70% ethanol for microCT analysis. Quantitative analysis of trabecular and cortical bone microarchitecture was performed by an investigator blinded to the sample genotypes. Fixed left femurs were scanned in 70% ethanol using a microCT 35 (Scanco Medical) with an X-ray tube with current of 0.1/0.18 mA and a peak energy of 50/60/70 kVp. Samples were scanned with a voxel size of 7 μm. Image segmentation used was 0.8 Sigma/1 Support /280 Threshold for trabecular scans and 0.8 Sigma/1 Support /320 Threshold for cortical scans. Trabecular bone analysis was performed on a 2.8 mm region starting 0.28 mm proximal to the growth plate. Identification of trabecular bone area was performed manually and drawn a few voxels away from the endocortical surface. Trabecular parameters were calculated using TRI-modeling.

Static Histomorphometry. Femurs were decalcified in 20% Ethylene-diaminetetraacetic acid for 2 wk, paraffin embedded, and longitudinally sectioned at 5 μm. Deparaffinization sections were stained for tartrate-resistant acid phosphatase (TRAP) activity (Sigma-Aldrich) and counterstained with 0.02% Fast

Green for osteoclast quantification (44). Measurements were taken using the Osteomeasure Analysis System (OsteoMetrics) in a region of interest 100 μm from the end of the growth plate extending 3 mm toward the midshaft. The percentage of osteoclast surface compared to total trabecular bone surface in the region of interest and the osteoclast number per bone surface were determined in two sections per sample and an average was obtained. Two sections per sample and total of six samples were used for analysis.

Osteoclastogenesis Assays. Bone marrow from male or female mice at either 8 wk or 6 mo of age was used for osteoclast differentiation assays using the adherent method. Bone marrow from femurs and tibiae was flushed with αMEM (Corning) and expanded on petri plastic plates for 3 d with 40 ng/mL macrophage colony-stimulating factor (M-CSF; R&D Systems). Following expansion, 25,000 adherent cells per 24 wells were plated in triplicate in the presence of osteoclast differentiation media (20 ng/mL M-CSF plus 10 ng/mL RANKL; R&D Systems) or 20 ng/mL M-CSF alone. Half of the media was replaced every 48 h with fresh osteoclast differentiation media. Following replating at indicated times, cells were fixed and stained for TRAP (Sigma) or Gill #3 (Sigma, M-CSF only cultures) for 30 s followed by washing with water. TRAP-expressing multinucleated cells (MNCs) containing three or more nuclei were identified as osteoclasts and manually quantified using an EVOS FlAuto scope (ThermoFisher). The total number of MNCs per 24 wells was quantified in each of the technical replicates averaged.

For IFNAR inhibition assays, Ultra-Leaf Purified anti-mouse IFNAR1 antibody (BioLegend, clone MAR1-5A3) or isotype control (Ultra-LEAF Purified Mouse IgG1, κ Isotype ctrl antibody, clone MOPC-21) was used. For differentiation studies, WT and SAVI cells were plated at 25,000 cells per 24 well as described above and cultured in M-CSF, RANKL, and 1 μg/mL isotype or IFNAR blocking antibody. Antibodies were replaced every 2 d, concurrent with addition of fresh differentiation media. For media studies, WT and SAVI cells were plated at 200,000 cells/24 well following 72 h of M-CSF differentiation as described above. These cells were cultured in differentiation media plus IFNAR1 antibody or isotype control at 5 μg/mL. The media were collected at d2 and replaced with fresh differentiation media and antibodies and cultured for an additional 2 d (d4). Secreted CCL5 (R&D DuoSet DY478-05) and CXCL10 (R&D Duo Set DY466-05) were measured by ELISA in the cultured media samples as indicated by the manufacturer with an extended standard curve.

Retroviral Infection of ISG15. Retroviral constructs pMx-HA-ISG15GG and pMx-HA-ISG15AA containing WT and mutant ISG15, respectively, were generated as previously described (45–47). For retroviral production, the above pMx-HA-ISG15 plasmids were transfected into PLAT-E cells (Cell biolabs, San Diego, CA) using Xtreme gene 9 (Roche, San Francisco, CA, USA) followed by collection of the virus-containing media for 48 h. The virus-containing media was then supplemented with polybrene (0.8 mg/mL) and used to transduce primary bone marrow macrophages in the presence of M-CSF. After 24 h, the media was replaced and cells were incubated with RANKL (50 ng/mL) and M-CSF (10 ng/mL) for 4 d (see detailed description in ref. (22)).

Osteoclast Differentiation and Cell RNA Isolation. RNA was extracted from cells lysed in TRIZOL (Invitrogen) using phenol-chloroform. Technical triplicates plated at 25,000 cells per well on day 0 were pooled to generate a single RNA sample. Samples were collected from RANKL-naïve cells (day 0) and from cells at days 2, 3, and 4 following RANKL stimulation.

qPCR. Reverse transcription was performed using purified RNA with the iScript cDNA Synthesis Kit (BioRad), according to the manufacturer's specifications. qPCR was performed using purchased primers (QuantiTect Primer Assays, Qiagen) and SYBR green-based detection. Fold changes were calculated using the $2^{-DDC(t)}$ method. At least three biologic replicates per genotype are reported.

RNA Sequencing. RNA from M-CSF-expanded WT and STING-deficient osteoclast cultures was tested for quality using an Agilent 2100 (Agilent RNA 6,000 Nano Kit) to determine RIN value, 28S/18S, and fragment length distribution. High-quality samples with RIN values greater than 7.5 and 28S/18S greater than 1.8 were used for sequencing. Libraries were constructed using nonstranded oligo dT library preps and sequenced at a depth of 50 bp for 20 million reads using a DNBSEQ platform (BGI Genomics). In total, 24 samples were analyzed (n = 3 per genotype at days 0 (pre-RANKL), and 2, 3, and 4 following RANKL stimulation). The sequenced samples were all derived from female mice. Reads from each sample were mapped to mouse mm10 reference genome using HISAT v2.0.5. Differential expression analyses between groups were performed using Cuffdiff (Cufflinks v2.2.1). Normalized counts of all the genes that were differentially expressed in at least one comparison group were used in downstream analyses and visualizations. Additional analysis was done with Qlucore Omics Explorer. These include a multigroup statistical analysis and generation of PCA analyses and heatmaps, and several gene lists were generated using noted *P*-value cutoffs of $P \leq 0.05$ or $P \leq 0.01$. *P*-values were determined using ANOVA with F-factor calculation. These gene lists were then used as input and compared to tonic and systemic ISG profiles of macrophages from ref. 11 for Venn Diagram creation using the Qlucore Omics explorer or subjected to pathway analysis using the ReactomePA package in R for visualization. RNA sequencing data was submitted and made publicly available using the Gene Expression Omnibus (GEO) platform (see below).

Western Blots. Immunoblots to assess the expression of STING protein were carried out on lysates derived from differentiating primary osteoclast precursor cells from C57BL/6 mice. Cell lysates were generated from bone marrow cultures expanded in 40 ng/mL M-CSF for 72 h. M-CSF precursors were plated in triplicate at 500,000 cells/well of a 6-well plate and cultured in the presence of 20 ng/mL M-CSF and 10 ng/mL RANKL for 1, 2, 3, or 4 d. For day 0 precursor samples, 1.5 × 10^6 cells were lysed after 72 h of 40 ng/mL M-CSF expansion. Cells were lysed using radio-immunoprecipitation assay buffer (RIPA) cell lysis buffer (Cell Signaling Technologies) and complete EDTA Protease inhibitors (Sigma-Aldrich). Equal amounts of protein were reduced and denatured by boiling in SDS-containing Laemmli buffer plus DTT and separated in 4 to 15% mini Protean gels (BioRad). Following transfer to polyvinylidene fluoride (PVDF), membranes were probed for STING (Cell Signaling, D1V5L), stripped using Restore Western Stripping Buffer (Thermo), and reprobed for β-actin (Cell Signaling, 8H10D10) according to the manufacturer's direction.

Statistics. Data were presented as mean ± SD. For each experiment, the Shapiro–Wilk test was applied to test for normal distribution of the data. If the data set passed normality, two-tailed unpaired Student's *t* tests were applied to compare two groups. If normality tests failed, two-tailed Mann–Whitney tests were used to compare between two groups. To compare more than two groups, ANOVA was used in datasets which passed Shapiro–Wilk tests, followed by Tukey and Bonferroni tests to correct for multiple comparisons. GraphPad PRISM (La Jolla, CA) was used for statistical analysis. $P < 0.05$ was considered statistically significant.

Data, Materials, and Software Availability. RNA sequencing data have been deposited in GEO (GSE226625, https://www.ncbi.nlm.nih.gov/geo/query/acc.cgi?acc=GSE226625) (48). All other data are shared in this article or in the accompanying *SI Appendix*.

ACKNOWLEDGMENTS. Support for this research was provided by research grants through the National Institutes of Health (E.M.G.: R01AR071037, S.S.: R01AI142005, S.M.: K01AR075896, K.A.F.: R01AI128358, Y.A.-A.: R01AR072623), by P30 AR075042 and by foundations (S.S.: Arthritis National Research Foundation, Arthritis and Aging Research Grant, K.A.F.: Lupus Research Alliance, Target Identification in Lupus Award). S.C. is a Netherlands Organization for Scientific Research Rubicon grant fellow.

Author affiliations: [a]Division of Rheumatology, Inflammation, and Immunity, Department of Medicine, Brigham and Women's Hospital, Boston, MA 02115; [b]Department of Immunology, Tufts University School of Medicine, Boston, MA 02111; [c]Department of Orthopedics and Cell Biology and Physiology, Washington University School of Medicine, Saint Louis, MO 63110; and [d]Department of Medicine, Program in Innate Immunity, University of Massachusetts Chan Medical School, Worcester, MA 01655

1. A. T. Shaw, E. M. Gravallese, Mediators of inflammation and bone remodeling in rheumatic disease. *Semin. Cell Dev. Biol.* **49**, 2–10 (2016).
2. W. J. Boyle, W. S. Simonet, D. L. Lacey, Osteoclast differentiation and activation. *Nature* **423**, 337–342 (2003).
3. V. Shalhoub *et al.*, Characterization of osteoclast precursors in human blood. *Br J. Haematol.* **111**, 501–512 (2000).
4. M. Pereira *et al.*, Common signalling pathways in macrophage and osteoclast multinucleation. *J. Cell Sci.* **131**, jcs216267 (2018).

5. K. Chen, J. Liu, X. Cao, Regulation of type I interferon signaling in immunity and inflammation: A comprehensive review. *J. Autoimmun.* **83**, 1–11 (2017).
6. H. Takayanagi *et al.*, RANKL maintains bone homeostasis through c-Fos-dependent induction of interferon-beta. *Nature* **416**, 744–749 (2002).
7. D. E. Place *et al.*, Osteoclast fusion and bone loss are restricted by interferon inducible guanylate binding proteins. *Nat. Commun.* **12**, 496 (2021).
8. F. Renner, M. L. Schmitz, Autoregulatory feedback loops terminating the NF-kappaB response. *Trends Biochem. Sci.* **34**, 128–135 (2009).
9. D. J. Gough, N. L. Messina, C. J. Clarke, R. W. Johnstone, D. E. Levy, Constitutive type I interferon modulates homeostatic balance through tonic signaling. *Immunity* **36**, 166–174 (2012).
10. L. B. Ivashkiv, L. T. Donlin, Regulation of type I interferon responses. *Nat. Rev. Immunol.* **14**, 36–49 (2014).
11. S. Mostafavi *et al.*, Parsing the interferon transcriptional network and its disease associations. *Cell* **164**, 564–578 (2016).
12. H. Ishikawa, G. N. Barber, STING is an endoplasmic reticulum adaptor that facilitates innate immune signalling. *Nature* **455**, 674–678 (2008).
13. D. R. E. Ranoa *et al.*, STING promotes homeostasis via regulation of cell proliferation and chromosomal stability. *Cancer Res.* **79**, 1465–1479 (2019).
14. M. Motwani, S. Pesiridis, K. A. Fitzgerald, DNA sensing by the cGAS-STING pathway in health and disease. *Nat. Rev. Genet.* **20**, 657–674 (2019).
15. M. Motwani *et al.*, Hierarchy of clinical manifestations in SAVI N153S and V154M mouse models. *Proc. Natl. Acad. Sci. U.S.A.* **116**, 7941–7950 (2019).
16. Y. Liu *et al.*, Activated STING in a vascular and pulmonary syndrome. *N. Engl. J. Med.* **371**, 507–518 (2014).
17. S. MacLauchlan, K. A. Fitzgerald, E. M. Gravallese, Intracellular sensing of DNA in autoinflammation and autoimmunity. *Arthritis Rheumatol.* **74**, 1615–1624 (2022).
18. C. E. Jacome-Galarza, S. K. Lee, J. A. Lorenzo, H. L. Aguila, Identification, characterization, and isolation of a common progenitor for osteoclasts, macrophages, and dendritic cells from murine bone marrow and periphery. *J. Bone Miner Res.* **28**, 1203–1213 (2013).
19. C. H. Choe *et al.*, Transmembrane protein 173 inhibits RANKL-induced osteoclast differentiation. *FEBS Lett.* **589**, 836–841 (2015).
20. Y. Kwon *et al.*, Cyclic dinucleotides inhibit osteoclast differentiation through STING-mediated interferon-beta signaling. *J. Bone Miner. Res.* **34**, 1366–1375 (2019).
21. V. Glatt, E. Canalis, L. Stadmeyer, M. L. Bouxsein, Age-related changes in trabecular architecture differ in female and male C57BL/6J mice. *J. Bone Miner. Res.* **22**, 1197–1207 (2007).
22. N. S. Adapala *et al.*, Inflammatory osteolysis is regulated by site-specific ISGylation of the scaffold protein NEMO. *Elife* **9**, e56095 (2020).
23. T. Takeuchi, G. Shimakawa, M. Tamura, H. Yokosawa, Y. Arata, ISG15 regulates RANKL-induced osteoclastogenic differentiation of RAW264 cells. *Biol. Pharm. Bull.* **38**, 482–486 (2015).
24. L. F. Coelho, G. Magno de Freitas Almeida, F. J. Mennechet, A. Blangy, G. Uze, Interferon-alpha and -beta differentially regulate osteoclastogenesis: Role of differential induction of chemokine CXCL11 expression. *Proc. Natl. Acad. Sci. U.S.A.* **102**, 11917–11922 (2005).
25. Z. Deng *et al.*, Def6 regulates endogenous type-I interferon responses in osteoblasts and suppresses osteogenesis. *Elife* **9**, e59659 (2020).
26. Q. Xiong, L. Zhang, W. Ge, P. Tang, The roles of interferons in osteoclasts and osteoclastogenesis. *Joint Bone Spine* **83**, 276–281 (2016).
27. J. H. Lee *et al.*, CXCL10 promotes osteolytic bone metastasis by enhancing cancer outgrowth and osteoclastogenesis. *Cancer Res.* **72**, 3175–3186 (2012).
28. H. B. Kwak *et al.*, Reciprocal cross-talk between RANKL and interferon-gamma-inducible protein 10 is responsible for bone-erosive experimental arthritis. *Arthritis Rheum.* **58**, 1332–1342 (2008).
29. S. M. Dai, K. Nishioka, K. Yudoh, Interleukin (IL) 18 stimulates osteoclast formation through synovial T cells in rheumatoid arthritis: Comparison with IL1 beta and tumour necrosis factor alpha. *Ann. Rheum. Dis.* **63**, 1379–1386 (2004).
30. H. Y. Yim *et al.*, Elevated response to type I IFN enhances RANKL-mediated osteoclastogenesis in Usp18-knockout mice. *J. Immunol.* **196**, 3887–3895 (2016).
31. B. Lin, Q. Ke, D. W. Leaman, V. Goel, A. Agarwal, Regulation of RANKL-induced osteoclastogenesis by RING finger protein RNF114. *J. Orthop. Res.* **36**, 159–166 (2018).
32. K. R. Loeb, A. L. Haas, The interferon-inducible 15-kDa ubiquitin homolog conjugates to intracellular proteins. *J. Biol. Chem.* **267**, 7806–7813 (1992).
33. O. Mirzalieva, M. Juncker, J. Schwartzenburg, S. Desai, ISG15 and ISGylation in human diseases. *Cells* **11**, 538 (2022).
34. R. Baum *et al.*, STING contributes to abnormal bone formation induced by deficiency of DNase II in mice. *Arthritis Rheumatol.* **69**, 460–471 (2017).
35. K. Kawane, H. Tanaka, Y. Kitahara, S. Shimaoka, S. Nagata, Cytokine-dependent but acquired immunity-independent arthritis caused by DNA escaped from degradation. *Proc. Natl. Acad. Sci. U.S.A.* **107**, 19432–19437 (2010).
36. K. Kawane *et al.*, Chronic polyarthritis caused by mammalian DNA that escapes from degradation in macrophages. *Nature* **443**, 998–1002 (2006).
37. H. Yoshida, Y. Okabe, K. Kawane, H. Fukuyama, S. Nagata, Lethal anemia caused by interferon-beta produced in mouse embryos carrying undigested DNA. *Nat. Immunol.* **6**, 49–56 (2005).
38. A. G. York *et al.*, Limiting cholesterol biosynthetic flux spontaneously engages type I IFN signaling. *Cell* **163**, 1716–1729 (2015).
39. H. Ishikawa, Z. Ma, G. N. Barber, STING regulates intracellular DNA-mediated, type I interferon-dependent innate immunity. *Nature* **461**, 788–792 (2009).
40. L. Jin *et al.*, MPYS is required for IFN response factor 3 activation and type I IFN production in the response of cultured phagocytes to bacterial second messengers cyclic-di-AMP and cyclic-di-GMP. *J. Immunol.* **187**, 2595–2601 (2011).
41. B. E. Clausen, C. Burkhardt, W. Reith, R. Renkawitz, I. Forster, Conditional gene targeting in macrophages and granulocytes using LysMcre mice. *Transgenic Res.* **8**, 265–277 (1999).
42. Y. S. Yang *et al.*, Bone-targeting AAV-mediated silencing of Schnurri-3 prevents bone loss in osteoporosis. *Nat. Commun.* **10**, 2958 (2019).
43. M. L. Bouxsein *et al.*, Ovariectomy-induced bone loss varies among inbred strains of mice. *J. Bone Miner. Res.* **20**, 1085–1092 (2005).
44. M. M. Matzelle *et al.*, Resolution of inflammation induces osteoblast function and regulates the Wnt signaling pathway. *Arthritis Rheum.* **64**, 1540–1550 (2012).
45. S. J. Jeon, K. C. Chung, Covalent conjugation of ubiquitin-like ISG15 to apoptosis-inducing factor exacerbates toxic stimuli-induced apoptotic cell death. *J. Biol. Chem.* **298**, 102464 (2022).
46. Y. L. Chen *et al.*, Interferon-stimulated gene 15 modulates cell migration by interacting with Rac1 and contributes to lymph node metastasis of oral squamous cell carcinoma cells. *Oncogene* **38**, 4480–4495 (2019).
47. Y. J. Jeon *et al.*, ISG15 modification of filamin B negatively regulates the type I interferon-induced JNK signalling pathway. *EMBO Rep.* **10**, 374–380 (2009).
48. S. Sharma, STING-dependent interferon signatures restrict osteoclast differentiation and bone loss in mice. *NCBI Gene Expression Omnibus*. https://www.ncbi.nlm.nih.gov/geo/query/acc.cgi?acc=GSE226625. Deposited 2 March 2023.